Science AAAS

First-Principles Calculations of PuO2±x

L. Petit, *et al.*

Science **301**, 498 (2003);
DOI: 10.1126/science.1086505

Science (print ISSN 0036-8075; online ISSN 1095-9203) is published weekly, except the last week in December, by the American Association for the Advancement of Science, 1200 New York Avenue NW, Washington, DC 20005.

provides an upper limit to the rate of serpentinization and yields a rate of 5.1×10^{-3} km^3/year (for 20% alteration of the massif). At this rate, it would take another 140,000 years to serpentinize the remaining volume of peridotite.

Independent of the degree of alteration in the Atlantis Massif, these calculations illustrate that the volume of peridotite is not the limiting factor in serpentinization-driven hydrothermal systems. In the absence of substantial conductive cooling, the amount of heat produced by serpentinization has the potential to drive moderate-temperature, Lost City–type systems for hundreds of thousands, if not millions, of years. The rate at which water is able to enter relatively cool mantle rocks ($<$425°C) (*17*, *19*), linked with tectonic activity, uplift rates, and crack permeabilities, are much more important in limiting the life of such systems. These processes in turn will influence conductive cooling and the efficiency of the system to transport heat released during serpentinization. Ultimately, temperature controls the rate of serpentinization. Rates are likely to be highest at temperatures of $\sim$250°C; hydration and diffusion rates are notably low below 100°C (*19*, *23*).

Our studies indicate that tectonic and hydrothermal processes at the LCHF are intimately linked and that they directly influence fluid-flow paths and the chemical and isotopic evolution of the fluids. Serpentinization and talc-metasomatism are a direct result of mantle denudation and most likely commenced close to the spreading center. Both processes are undoubtedly ongoing below the vent field. As the system evolved, a number of self-propagating mechanisms increased permeability and fluid access that may ultimately be crucial for the formation of such vent fields. For example, along the southern scarps of the massif, complex networks of steeply dipping faults, fracturing, and mass wasting are driven by fracture-zone tectonics and alteration-induced volumetric expansion (*1*, *9*). This enhances exfoliation along the scarp, penetration of seawater into the relatively cool, fresh peridotite, and propagation of the serpentinization front toward the north into the central dome of the massif. In addition, diffusely percolating, high-pH fluids emanating from the underlying serpentinites promote rapid sediment lithification (*1*, *6*), which offers an efficient mechanism for slowing heat loss and maintaining higher temperatures in the basement. Collectively these processes have the potential to prolong hydrothermal activity for tens of thousands of years. If high-pH, reducing, ultramafic systems are analogous to early Earth environments, the LCHF provides a natural laboratory to understand the links between serpentinization, carbonate precipitation, and microbial activity in ancient ecosystems (*6*).

References and Notes

1. D. S. Kelley *et al.*, *Nature* **412**, 145 (2001).
2. M. E. Berndt, D. E. Allen, W. E. Seyfried Jr., *Geology* **24**, 351 (1996).
3. M. O. Schrenk, P. Cimino, D. S. Kelley, J. A. Baross, *Eos* **83**, F2301 (abstr. B71B-0742) (2002).
4. G. MacLeod, C. McKeown, A. J. Hall, M. J. Russell, *Orig. Life Evol. Biosph.* **23**, 19 (1994).
5. E. L. Shock, M. D. Schulte, *J. Geophys. Res.* **103**, 28513 (1998).
6. D. S. Kelley, J. A. Baross, G. L. Früh-Green, M. O. Schrenk, J. A. Karson, *Eos.* **83**, F222 (abstr. B62A-03) (2002).
7. D. K. Blackman, J. R. Cann, B. Janssen, D. K. Smith, *J. Geophys. Res.* **103**, 21315 (1998).
8. J. R. Cann *et al.*, *Nature* **385**, 329 (1997).
9. D. K. Blackman *et al.*, *InterRidge News* **10.1**, 33 (2001); available online at http://triton.ori.utokyo.ac.jp/~intridge/irn-toc01.htm#101.
10. Thermodynamic calculations with the program PHREEQE (*12*) indicate that seawater is undersaturated with respect to brucite, in contrast to supersaturation of brucite, talc, and serpentine for mixing of seawater with the range of vent fluid compositions reported by (*1*).
11. D. L. Parkhurst, D. C. Thorstenson, L. N. Plummer, *U.S. Geological Survey Water-Resources Investigations Report 80-96* (1980).
12. Materials and methods are available as supporting material on *Science* Online.
13. 1973 GEOSECS ^{14}C data for Station 117, the closest to LCHF, indicate Δ^{14}C values of –32.2 and –67.9 at depths of 686 and 1076, respectively, and correspond to reservoir ages of 268 and 565 years, respectively. The young ages of the active vents suggest that bomb radiocarbon has penetrated deeper into the water column and that the vents must be fed by relatively shallow water masses. If recharge of the hydrothermal system was deep water, ages of at least 830 years (reservoir age at $\sim$30°N) would be obtained. More information can be found online at http://iridl.ldeo.columbia.edu/SOURCES/GEOSECS/.
14. L. D. Stott, C. M. Tang, *Paleooceanography* **11**, 37 (1996).
15. G. S. Schmidt, G. R. Bigg, E. J. Rohling, Global Seawater Oxygen-18 Database (1999); available online at www.giss.nasa.gov/data/o18data/.
16. D. P. Schrag *et al.*, *Quat. Sci. Rev.* **21**, 331 (2002).
17. G. L. Früh-Green, J. A. D. Connolly, A. Plas, D. S. Kelley, B. Grobéty, in *The Subseafloor Biosphere at Mid-Ocean Ridges*, W. D. Wilcock, D. S. Kelley, E. DeLong, C. Cary, Eds. (American Geophysical Union, Washington, DC, in press).
18. W. S. Fyfe, P. Lonsdale, in *The Sea*, C. Emiliani, Ed. (Wiley, New York, 1981), vol. 7, pp. 589–638.
19. A. H. Macdonald, W. S. Fyfe, *Tectonophysics* **116**, 123 (1985).
20. R. S. Detrick, J. A. Collins, *Eos* **79**, F800 (1998).
21. S. L. Nooner, G. S. Sasagawa, D. K. Blackman, M. A. Zumberge, *Geophys. Res. Lett.* **30**, 1446 (2003).
22. R. P. Lowell, P. A. Rona, *Geophys. Res. Lett.* **29**, 10.1029/2001GL01411 (2002).
23. B. Martin, W. S. Fyfe, *Chem. Geol.* **6**, 185 (1970).
25. We thank I. Hajdas (ETH) and T. Brown [Center for Accelerator Mass Spectrometry (CAMS)] for ^{14}C-age dating, E. William for evaluation of sea-floor imagery, and B. Nelson for Sr measurements. We acknowledge funding from ETH grant 0-20890-01 to G.L.F.-G. and from NSF grants OCE97-12549 to D.S.K. and OCE97-12430 to J.A.K. G.P. was in part supported by NSF and the CAMS at Lawrence Livermore National Laboratory through the University Collaborative Research Program.

Supporting Online Material

www.sciencemag.org/cgi/content/full/301/5632/495/DC1
Materials and Methods
SOM Text
Fig. S1
References and Notes

11 April 2003; accepted 19 June 2003

First-Principles Calculations of $PuO_{2\pm x}$

L. Petit,[1,2] A. Svane,[1]* Z. Szotek,[3] W. M. Temmerman[3]

The electronic structure of $PuO_{2\pm x}$ was studied using first-principles quantum mechanics, realized with the self-interaction corrected local spin density method. In the stoichiometric PuO_2 compound, Pu occurs in the Pu(IV) oxidation state, corresponding to a localized f^4 shell. If oxygen is introduced onto the octahedral interstitial site, the nearby Pu atoms turn into Pu(V) (f^3) by transferring electrons to the oxygen. Oxygen vacancies cause Pu(III) (f^5) to form by taking up electrons released by oxygen. At $T = 0$, the PuO_2 compound is stable with respect to free oxygen, but the delicate energy balance suggests the possible deterioration of the material during long-term storage.

Although Pu oxidizes readily, until recently it was accepted wisdom that PuO_2 is the chemically stable Pu oxide (*1*); showing no sign of reaction when exposed to air, it was the compound of choice for the long-term storage of Pu. The discovery by Haschke *et al.* (*2*) of higher composition binary oxides, PuO_{2+x} ($x \leq 0.27$), might therefore have wide-ranging implications (*3*,*4*). The oxidation reaction was found to occur in the presence of water, $PuO_2 + xH_2O \rightarrow PuO_{2+x} + xH_2$, at temperatures in the range of 25° to 350°C. Nevertheless, despite considerable experimental evidence, the existence of PuO_{2+x} remains controversial (*5*), because many earlier attempts to prepare oxides containing Pu atoms with oxidation states above 4 have failed.

We studied changes in the Pu f-electron configuration induced by the oxidation/reduction process from PuO_2 to PuO_{2+x}/PuO_{2-x}, based on ab initio electronic structure

---

[1] Department of Physics and Astronomy, University of Aarhus, DK-8000 Aarhus C, Denmark. [2] Computer Science and Mathematics Division, and Center for Computational Sciences, Oak Ridge National Laboratory, Oak Ridge, TN 37831–6114, USA. [3] Daresbury Laboratory, Daresbury, Warrington WA4 4AD, UK

*To whom correspondence should be addressed. E-mail: svane@phys.au.dk

calculations that were performed using the self-interaction corrected (SIC) local spin density (LSD) approximation. The quantum mechanical modeling of Pu and Pu compounds poses a special challenge because of the position of this element in the actinide series. The earlier actinides (Th, Pa, U, and Np) are dominated by the itinerant (delocalized) behavior of the 5f electrons; the later actinides (Am, Cm, Bk, Cf, and Es) are characterized by localized 5f electrons, which do not contribute to the bonding in the solid phase. Depending on chemical surroundings, Pu may exhibit more or less localized character. We modeled this phenomena with the SIC-LSD approach by describing some of the f electrons as localized and others as delocalized. The energetics of the chemical bonding to the ligands determines the most favorable way to split the f-electron manifold and allows for an interpolation between the fully localized and fully delocalized limits. In the SIC-LSD approach, the Pu oxidation state is given as the number of electrons available for band formation, and a change in Pu oxidation state is manifested as a localization-delocalization transition in the f-electron manifold. We find that the oxidation state of Pu in PuO_2 readily increases or decreases upon addition or removal of O, respectively, which suggests a possible existence of high composition binary oxides of Pu.

PuO_2 crystallizes in the cubic fluorite (CaF_2) structure, with a lattice parameter of a_0 = 5.396 Å, at 25°C (*5*). Stoichiometric PuO_2 is an insulator, with the assumed ground-state configuration of the Pu ion being $5f^4$; i.e., in the solid, four f electrons are localized on each Pu site. Electronic structure calculations, based on a delocalized description of the f electrons in PuO_2, predict metallic behavior with the appearance of narrow f band at the Fermi level, E_F. This is in disagreement with the insulating behavior of PuO_2. Treating the 5f electrons as atomic-like states (*6*, *7*) results in a lattice constant that is in good agreement with experiment and a density of states (DOS) that can explain the insulating character of PuO_2, thus confirming the localized nature of the f electrons.

Rather than determining the f-electron configuration from a comparison to empirical data, the SIC-LSD method is entirely ab initio and relies on total energy considerations. Both localized and delocalized f electrons are treated equally (*8*), but with the inclusion of an explicit energy contribution for an electron localization (the self-interaction correction) (*9*). The method has previously been applied succesfully to many systems and, among them, both lanthanide (*10*) and actinide (*11*) compounds. By comparing the total energies for different localized Pu f^n configurations, the ground-state configuration can be deduced from the absolute minimum in the total energy. For PuO_2, the SIC-LSD total energies as functions of volume have been calculated for the localized $5f^5$, $5f^4$, and $5f^3$ configurations, as well as for the fully itinerant f^0 configuration (Fig. 1). The tetravalent $5f^4$ configuration is indeed seen to be the global energy minimum, with the corresponding lattice constant of 5.34 Å, in good agreement with experiment. Localization of only three f electrons per Pu atom leads to a modestly higher energy (6 mRy per formula unit), demonstrating the volatility of the Pu f^4 shell. In contrast, with five localized f electrons on each Pu, the energy is 110 mRy higher than the f^4 ground state, effectively ruling out this as a realistic model of PuO_2.

To study the electronic structure of PuO_{2+x}, with $x = 0.25$, a periodic supercell consisting of four PuO_2 formula units (Fig. 2) has been used, constituting the conventional fluorite cubic cell of Pu_4O_8. To realize this high level of doping, an additional O atom (O impurity) was placed on the octahedral interstitial site, giving rise to a hypothetical Pu_4O_9 compound. The x-ray and neutron diffraction data confirm that PuO_{2+x} indeed has a fluorite related face-centered cubic structure and that the extra O atoms are accommodated on the interstitial sites of PuO_2 (*2*). The inclusion of the extra O atom into the fluorite lattice has a profound effect on the calculated electronic structure, as can be seen from a comparison of the DOS in the valence and conduction bands of $Pu_4^{4+}O_8$ and $Pu_4^{4+}O_9$ (Fig. 3, A and B, respectively). [The 4+ superscript for both compounds indicates that the Pu ions are all assumed to be in the tetravalent f^4 configuration, Pu(IV).] In the case of Pu_4O_9, a broad band that originates from the p-p and p-f overlap between interstitial O atoms and their O and Pu neighbors spans the energy range where, in Pu_4O_8, the insulating gap (theoretical value, 0.94 eV) is situated. The position of E_F indicates that this impurity-derived p band is only partially filled, which arises because only four valence p states of the added O atom are occupied.

To what extent would it be favorable to populate further these O impurity p band states by delocalizing f electrons on the neighboring Pu atoms? To address this point, we present the DOS for a scenario with two additional f electrons delocalized, that is, two of the neighboring Pu atoms have the $5f^3$ localized configuration (Fig. 3C). We refer to this configuration as $Pu_2^{5+}Pu_2^{4+}O_9$. From Fig. 3C, it follows that the two extra itinerant electrons (compared with Fig. 3B) are indeed accommodated in the O impurity p band, as a result of charge transfer and Pu-O hybridization, indicated by the upward shift of E_F. The delocalized f states give rise to an additional narrow f peak, which occurs above E_F and thus remains unoccupied. Whether the delocalization is energetically favorable depends on the gain in electrostatic and kinetic energies caused by this rearrangement of charge, which must be large enough to overcome the associated loss in localization (self-interaction correction) energy. This situation indeed is the case, as can be seen from Fig. 4, which shows the total energies and corresponding theoretical equilibrium lattice parameters for various 5f-electron configurations of the hypothetical compound Pu_4O_9. The largest change in energy, $\Delta E = -54$ mRy, occurs when a single f electron becomes delocalized ($Pu^{5+}Pu_3^{4+}O_9$), with respect to the original tetravalent configuration ($Pu_4^{4+}O_9$). A consid-

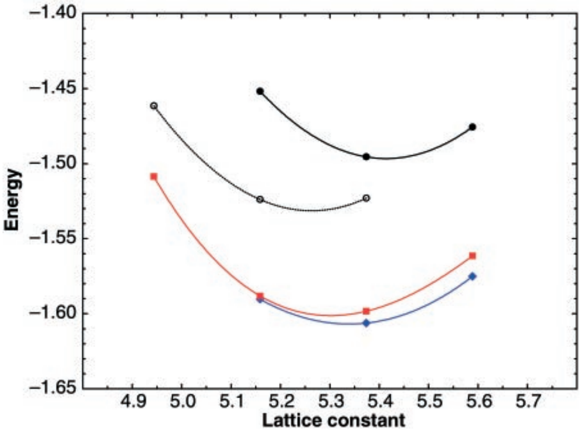

Fig. 1. Total energy versus lattice parameter for PuO_2 assuming different localized f shells on Pu. f^0, all f electrons are treated as delocalized band states (black dotted line); f^3 (red line); f^4 (blue line); and f^5 (black solid line) corresponding to the Pu(V), Pu(IV), and Pu(III) oxidation states, respectively. Units are Rydberg for the energy (relative to the energy of the free neutral atoms) and Å for the lattice constant, both per formula unit.

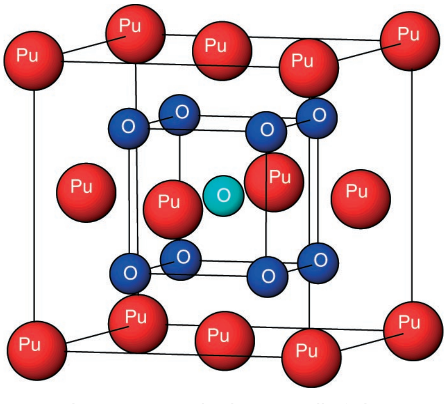

Fig. 2. The conventional cubic unit cell of plutonium dioxide in the fluorite structure. The cube contains four PuO_2 units (red Pu and dark blue O atoms). The central O atom (cyan) marks the octahedral interstitial position, where excess O in PuO_{2+x} is accommodated. The modeling of $PuO_{2.25}$ is facilitated by occupying the central position in all cubic units. Similarly, the oxygen-deficient $PuO_{1.75}$ compound is modeled by leaving one of the dark blue O sites vacant in addition to the central interstitial site.

erable gain in energy, $\Delta E = -21$ mRy, is also observed when delocalizing a further electron on a second Pu atom ($Pu_2^{5+}Pu_2^{4+}O_9$), indicating that the filling of the O impurity p states, by depopulating Pu f states, is associated with a large gain in charge transfer and hybridization energy. The energy gains for delocalizing also the third ($Pu_3^{5+}Pu^{4+}O_9$) and fourth ($Pu_4^{5+}O_9$) f electrons are small, respectively 1.6 and 1.2 mRy per PuO_{2+x} formula unit. With the p band being filled by the first two delocalized electrons, these last two electrons start filling the narrow f peak (Fig. 3D). The corresponding gain in band formation energy is small, essentially balancing out the loss in SIC energy, within the accuracy of the method.

The total gain in energy due to f-electron delocalization is $E_{Pu^{5+}O_{2.25}} - E_{Pu^{4+}O_{2.25}} = -22$ mRy. The main difference between Pu_4O_8 and Pu_4O_9 is that in Pu_4O_8 the extra p band is not present, and any delocalized f electron will have to be accommodated in the narrow f bands above the band gap. The gain in band formation energy associated with this transfer is not large enough to overcome the loss in localization energy, and the f electrons prefer to remain localized. Thus, in our approach Pu_4O_8 is insulating, while Pu_4O_9 is metallic. The localized and delocalized behaviors nearly balancing out for the third and fourth Pu f electrons may be taken as an indication that the true state is intermediate between the Pu^{4+} and Pu^{5+} which means that, on any Pu site, the Pu ion fluctuates between these configurations in a correlated way, so that at least two Pu^{5+} sites are present among the O impurity neighbors. A similar picture of Ce fluctuating between f^1 and f^0 in the vicinity of O vacancies in CeO_2 has been conjectured by Skorodumova *et al.* (*12*).

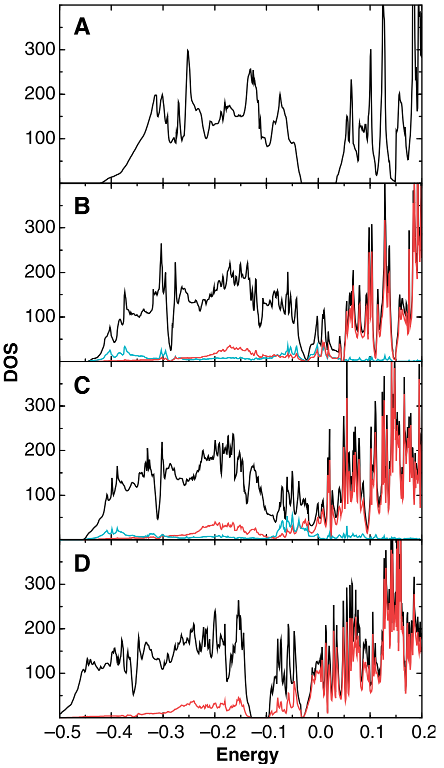

Fig. 3. Total density of states (black), Pu f-projected DOS (red) and interstitial O p-projected DOS (blue) for (**A**) the tetravalent $Pu_4^{4+}O_8$ compound, (**B**) the tetravalent $Pu_4^{4+}O_9$ compound, (**C**) the mixed $Pu_2^{5+}Pu_2^{4+}O_9$ compound, and (**D**) the pentavalent $Pu_4^{5+}O_9$ compound. The interstitial O DOS is only displayed in (B) and (C). The energy (in Rydberg) is relative to E_F.

It follows from our calculations that the O insertion into PuO_2 increases the Pu oxidation state beyond four. The calculated pentavalent ground-state configuration for PuO_{2+x} is in agreement with the latest extended x-ray absorption fine structure results (*13*), which indicate the presence of Pu^{5+} ions. Initial x-ray photoemission spectroscopy data (*14*) suggested that, after the inclusion of the O into PuO_2, some of the Pu^{4+} ions were replaced by Pu^{6+} ions. In the SIC-LSD approach, this process translates into delocalizing two f electrons from the same Pu ion, leading to the formation of $Pu^{6+}Pu_3^{4+}O_9$, which from our calculations is energetically unfavorable with respect to any of the previously studied delocalization scenarios (Fig. 4). The strong on-site f-f correlations that are involved when delocalizing a second electron on the same Pu site cannot be overcome by gain in hybridization energy.

Measurements reveal that the accommodation of extra O in the fluorite structure leads to a vanishingly small increase in the lattice parameter *a* (*2*). Thus, for $PuO_{2.265}$ a lattice parameter of 5.404 Å is obtained, compared with 5.397 Å for PuO_2. This change of the lattice parameter during the PuO_{2+x} formation does not happen in a continuous manner, and about half of it is realized in an initial step as *x* first exceeds 0 (*2*). The apparent insensitivity of the lattice parameter to O inclusion was explained by the combined effect of the expansion of the lattice due to additional O and the shrinking of the lattice due to the replacement of the tetravalent Pu ion by higher oxidation-state Pu cations. The theoretical equilibrium lattice parameters for different Pu configurations (Fig. 4) confirm this assertion. In particular, the calculated lattice parameter for $Pu_4^{4+}O_8$ is 5.34 Å, whereas the minimum of the total energy for $Pu_4^{4+}O_9$ occurs at $a = 5.37$ Å. As expected, the inclusion of an extra O atom has led to the expansion of the fluorite lattice. Subsequently, when the Pu f electrons are gradually delocalized (configurations $Pu^{5+}Pu_3^{4+}O_9$ through $Pu_4^{5+}O_9$), the lattice parameter decreases slightly, as a result of the increasing number of bonding electrons. The combined effect of these two trends is a lattice constant that is almost unchanged with respect to the lattice constant of Pu_4O_8, in agreement with experiment by Haschke *et al.*(*2*) and their conjecture. On balance, our calculations find the lattice constant of $PuO_{2.25}$ slightly smaller than that of PuO_2, whereas experiment finds it slightly higher. This difference may indicate the presence of dynamical correlations in the narrow band formed by the f electrons that have been delocalized and for which the static band treatment could have led to an overestimation of their bonding contribution. This interpretation is suggested by the decreasing lattice parameter after oxidation of the slightly less correlated UO_2 compound (*2*). The larger spatial extent of the f orbitals of U compared with Pu results in more substantive energy gains, due to increased hybridization, in U compounds compared with Pu compounds, which leads to smaller lattice constants. The observation (*15*) of U^{6+} ions in UO_{2+x} is a direct indication of reduced correlations among the delocalized U f electrons in comparison to the Pu f electrons, which result in larger fluctuations in the U f occupancies.

When oxygen atoms are removed from PuO_2 to form O-deficient compounds PuO_{2-x},

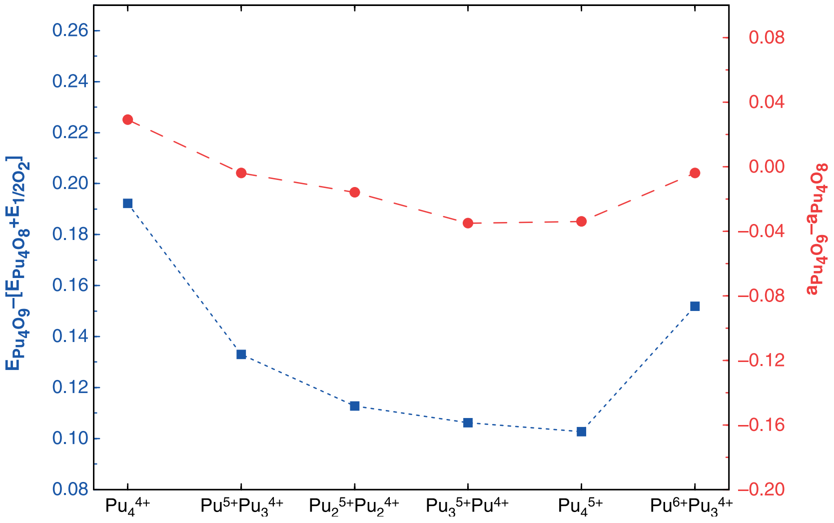

Fig. 4. Total energy minima (blue, and left-side axis) and corresponding theoretical equilibrium lattice constants (red, and right-side axis) for different Pu f configurations of Pu_4O_9. The energy (in Ry units) and lattice parameter data (in Å units) are given with respect to the corresponding values for $Pu_4O_8+[1/2]O_2$.

noticeable changes in lattice parameter are observed (*16*). For $PuO_{1.87}$, for example, a lattice parameter of 5.446 Å is measured: an increase of 0.9 % with respect to the lattice constant of stoichiometric PuO_2. Here, we have studied the electronic structure of $PuO_{1.75}$. Starting again from the unit cell shown (Fig. 2), the Pu_4O_7 supercell has been constructed by removing one of the eight O atoms (marked in dark blue). We subsequently calculated the total energy as a function of lattice parameter, both for the tetravalent ${Pu_4}^{4+}O_7$ and for the trivalent ${Pu_4}^{3+}O_7$ configurations; the latter has been found to be the ground-state solution. Compared with Pu_4O_8, we find that the removal of an O atom results in the localization of one further f electron on each of the Pu sites, i.e., the opposite trend to adding O atom to the PuO_2 compound. The increased degree of f-electron localization leads to a distinct increase in the calculated lattice parameter, a_0 = 5.558 Å, as the bonding O p electrons are removed and replaced with nonbonding localized Pu f electrons.

The foregoing discussion implies that the increase or decrease in the Pu state of oxidation under O insertion to or extraction from PuO_2 can be explained in terms of a localization/delocalization transition by correcting for the self-interaction associated with the strongly correlated 5f electrons. Whether the oxidation process actually takes place depends on the thermodynamic conditions, in particular the chemical potential of the additional oxygen. We are not able to calculate the entropic contributions to the free energy here; however the total energy balance of the reaction

$$\mathrm{PuO_2} + \tfrac{1}{8}\mathrm{O_2} \rightleftharpoons \mathrm{PuO_{2.25}} \qquad (1)$$

finds the reduction (left side) to be more favorable by 25 mRy (using an LSD binding energy of the free O_2 molecule of 0.7 Ry). Thus, at $T = 0$ the dioxide is stable, in agreement with the observed chemical stability of this compound. Depending on actual conditions (temperature and chemical potential of oxygen), it is conceivable that the oxidation may become favorable, given the small energy barrier. The experimental oxidation process of (*2*) uses H_2O as oxidant, at 32 mbar H_2O pressure and at temperatures between 25° and 350°C. In this case oxidation is accompanied by production of H_2, which is favored by high entropy.

This study of the electronic structure of PuO_{2+x} did not consider such complex species as O_2^- and O_2^{2-} as possible candidates for the extra O. Similarly, noncubic distortions of the O sublattice were not considered, although such configurations are often encountered in oxide systems (*15*). The relevance of these issues in PuO_{2+x} compounds depends strongly on the energy considerations with respect to the independent interstitial O. The important outcome of this work is that Pu ions play an active role in accommodating extra O in the PuO_2 matrix, because their localized f states act as electron reservoirs for the O^{2-} ions: for *x* greater than 0, the added O impurities absorb electrons released by the neighbouring Pu(IV) ions in the process of f-electron delocalization leading to the formation of Pu(V) ions. A recent model of corrosion of Pu (*17*) assumes an analogous situation. Similarly, when O atoms are removed from stoichiometric PuO_2, the extra electrons are absorbed in the formation of Pu(III) ions, with the localized f^5 configuration, in the vicinity of O vacancies. We find PuO_2 energetically stable with respect to interactions with free O_2 molecules, consistent with the results from decades of research on this subject. The properties of PuO_{2+x} predicted by our calculations also agree very well with the experimental findings by Haschke *et al.* (*2*). Thus, higher oxidation states may be possible under specific experimental or even environmental conditions. Pu oxidation states of 6 and above have not been found in PuO_{2+x}, but may be realizeable in more exotic circumstances (*18*).

References and Notes

1. F. Weigel, J. J. Katz, G. T. Seaborg, in *The Chemistry of the Actinide Elements*, J. J. Katz, G. T. Seaborg, L. R. Morss, Eds. (Chapman & Hall, New York, 1986), vol. 1, p. 680.
2. J. M. Haschke, T. H. Allen, L. A. Morales, *Science* **287**, 285 (2000).
3. C. Madic, *Recherche* **330**, 22 (2000).
4. J. Haschke, T. H. Allen, *J. Alloys Comp.* **336**, 124 (2002).
5. R. G. Haire, J. M. Haschke, *MRS Bull. 689* (September 2001).
6. P.J. Kelly, M. S. S. Brooks, *J. Chem. Soc. Faraday Trans. 2* **83**, 1189 (1987).
7. M. Colarieti-Tosti, O. Eriksson, L. Nordström, J. Wills, M. S. S. Brooks, *Phys. Rev. B* **65**, 195102 (2002).
8. W. M. Temmerman, A. Svane, Z. Szotek, H. Winter, in *Electronic Density Functional Theory: Recent Progress and New Directions*, J. F. Dobson, G. Vignale, M. P. Das, Eds. (Plenum, New York, 1998), p. 327.
9. J. P. Perdew, A. Zunger, *Phys. Rev. B* **23**, 5048 (1981).
10. P. Strange, A. Svane, W. M. Temmerman, Z. Szotek, H. Winter, *Nature* **399**, 756 (1999).
11. L. Petit, A. Svane, W. M. Temmerman, Z. Szotek, *Phys. Rev. Lett.* **88**, 216403 (2002).
12. N. V. Skorodumova, S. I. Simak, B. I. Lundqvist, I. A. Abrikosov, B. Johansson, *Phys. Rev. Lett.* **89**, 166601 (2002).
13. L. A. Morales, J. M. Haschke, T. H. Allen, *Am. Inst. Phys.* **532**, 114 (2000).
14. J. M. Haschke, T. H. Allen, Report LA-13537, Los Alamos, NM (1999).
15. C. A. Colmenares, *Prog. Solid State Chem.* **9**, 139 (1975).
16. E. R. Gardner, T. L. Markin, R. S. Street, *J. Inorg. Nucl. Chem.*, **27**, 541 (1965).
17. J. M. Haschke, T. H. Allen, L. A. Morales, *J. Alloys Comp.* **314**, 78 (2001).
18. M. Straka, K. G. Dyall, P. Pyykkö, *Theor. Chem. Acc.* **106**, 393 (2001).
19. Partially funded by the European Union Training and Mobility in Research and Research Training Networks (contracts: FMRX-CT98-0178 and HPRN-CT-2002-00295). Work supported by the Defense Advanced Research Project Agency and by the DOE Office of Science through Basic Energy Services/Division of Materials Science and Engineering under Contract No. DE-AC05-00OR22725 with UT-Battelle LLC.

6 May 2003; accepted 25 June 2003

The Archaeology of Ushki Lake, Kamchatka, and the Pleistocene Peopling of the Americas

Ted Goebel,[1]* Michael R. Waters,[2] Margarita Dikova[3]

The Ushki Paleolithic sites of Kamchatka, Russia, have long been thought to contain information critical to the peopling of the Americas, especially the origins of Clovis. New radiocarbon dates indicate that human occupation of Ushki began only 13,000 calendar years ago—nearly 4000 years later than previously thought. Although biface industries were widespread across Beringia contemporaneous to the time of Clovis in western North America, these data suggest that late-glacial Siberians did not spread into Beringia until the end of the Pleistocene, perhaps too recently to have been ancestral to proposed pre-Clovis populations in the Americas.

Anthropologists have long looked to Siberia for the origins of the first Americans. Much attention has focused on the search for an immediate antecedent of Clovis (*1–3*), the earliest unequivocal complex of archaeological sites in North America (*4*). A clear connection between the Siberian Paleolithic and early American sites, however, continues to be elusive.

One Siberian locality pivotal to understanding the peopling of the Americas is the site complex around Ushki Lake, Kamchatka (Fig. 1). Ushki Lake is located in the maritime region of southwestern Beringia, 55°N latitude. Dikov excavated the Ushki sites from 1964 through 1990, revealing two late Paleolithic cultural components in a stratified

---

[1] Department of Anthropology/096, University of Nevada Reno, Reno, NV 89557, USA. [2] Department of Anthropology, Texas A&M University, College Station, TX 77843–4352, USA. [3] Laboratory of Archaeology, Northeast Asian Interdisciplinary Research Science Center, Russian Academy of Sciences, Magadan, Russia.

*To whom correspondence should be addressed. E-mail: goebel@unr.edu